

The origin of the conductivity maximum in molten salts. II. SnCl_2 and HgBr_2

Nikhil P. Aravindakshan, Colin M. Kuntz, Kyle E. Gemmell, Keith E. Johnson, and Allan L. L. East

Citation: *The Journal of Chemical Physics* **145**, 094504 (2016); doi: 10.1063/1.4961687

View online: <http://dx.doi.org/10.1063/1.4961687>

View Table of Contents: <http://scitation.aip.org/content/aip/journal/jcp/145/9?ver=pdfcov>

Published by the AIP Publishing

Articles you may be interested in

[A theoretical study of \$\text{SnF}_2^+\$, \$\text{SnCl}_2^+\$, and \$\text{SnO}_2^+\$ and their experimental search](#)

J. Chem. Phys. **137**, 154302 (2012); 10.1063/1.4758475

[Temperature dependent conductivity of polycrystalline \$\text{Cu}_2\text{ZnSnS}_4\$ thin films](#)

Appl. Phys. Lett. **100**, 263903 (2012); 10.1063/1.4731875

[The origin of the conductivity maximum in molten salts. I. Bismuth chloride](#)

J. Chem. Phys. **136**, 124504 (2012); 10.1063/1.3694830

[Optical properties of \$\text{SnCl}_2\$ phosphor](#)

J. Appl. Phys. **109**, 083539 (2011); 10.1063/1.3576118

[A systematic ab initio study of the structure and vibrational spectroscopy of \$\text{HgCl}_2\$, \$\text{HgBr}_2\$, and \$\text{HgBrCl}\$](#)

J. Chem. Phys. **119**, 12271 (2003); 10.1063/1.1624828



NEW Special Topic Sections

NOW ONLINE
Lithium Niobate Properties and Applications:
Reviews of Emerging Trends

AIP | Applied Physics
Reviews

The origin of the conductivity maximum in molten salts. II. SnCl_2 and HgBr_2

Nikhil P. Aravindakshan, Colin M. Kuntz, Kyle E. Gemmell, Keith E. Johnson, and Allan L. L. East^{a)}

Department of Chemistry and Biochemistry, University of Regina, Regina, Saskatchewan S4S 0A2, Canada

(Received 9 June 2016; accepted 15 August 2016; published online 2 September 2016)

The phenomenon of electrical conductivity maxima of molten salts versus temperature during orthobaric (closed-vessel) conditions is further examined via *ab initio* simulations. Previously, in a study of molten BiCl_3 , a new theory was offered in which the conductivity falloff at high temperatures is due not to traditional ion association, but to a rise in the activation energy for atomic ions hopping from counterion to counterion. Here this theory is further tested on two more inorganic melts which exhibit conductivity maxima: another high-conducting melt (SnCl_2 , $\sigma_{\text{max}} = 2.81 \Omega^{-1} \text{cm}^{-1}$) and a low-conducting one (HgBr_2 , $\sigma_{\text{max}} = 4.06 \times 10^{-4} \Omega^{-1} \text{cm}^{-1}$). First, *ab initio* molecular dynamics simulations were performed and again appear successful in reproducing the maxima for both these liquids. Second, analysis of the simulated liquid structure (radial distributions, species concentrations) was performed. In the HgBr_2 case, a very molecular liquid like water, a clear *Grotthuss chain of bromide transfers* was observed in simulation when seeding the system with a HgBr^+ cation and HgBr_3^- anion. The first conclusion is that the hopping mechanism offered for molten BiCl_3 is simply the Grotthuss mechanism for conduction, applicable not just to H^+ ions, but also to halide ions in post-transition-metal halide melts. Second, it is conjectured that the conductivity maximum is due to rising activation energy in network-covalent (halide-bridging) melts (BiCl_3 , SnCl_2 , PbCl_2), but possibly a falling Arrhenius prefactor (collision frequency) for molecular melts (HgBr_2). Published by AIP Publishing. [<http://dx.doi.org/10.1063/1.4961687>]

I. INTRODUCTION

Molten salts have many desirable properties, including good electrical conductivity, high thermal stability, low viscosity, low vapour pressure, and nonflammability.^{1,2} As electrolytes, molten salts are used in electrolytic cells for (i) electrodeposition, electro-oxidation, electro-deoxidation, and electrosynthesis;³⁻⁷ (ii) thermally activated batteries (thermal batteries), which are primarily used for military applications;⁸ and (iii) prototype liquid metal batteries for low-cost and low-temperature grid-scale electricity storage.^{9,10} Although the past few decades have shown more research interest in ionic liquids (organic salts which melt below 100°C) rather than traditional molten salts, Johnson^{11,12} has pointed out that ionic liquids have structural and conductivity issues that might be best explored by readdressing similar issues with classical molten salts, which ionise as atomic or molecular ions, show a wide range of conductivity values (10^{-8} – $10^1 \Omega^{-1} \text{cm}^{-1}$), and hence open a broader window to explore different conductivity mechanisms.

In the 1960s, Yosim and Grantham studied the electrical conductivities of several “covalent” molten salts, such as CuCl , BiCl_3 , SnCl_2 , and HgBr_2 , at elevated temperatures under orthobaric conditions (sealed under vacuum).¹³⁻¹⁶ They found that there is a maximum in specific conductivity vs temperature for at least 11 of these and proposed that such maxima would exist with all fluids at sufficiently high temperature and sufficiently reduced density.¹⁴ They attributed the conductivity

decline at high temperatures to increased ion association (loss of ions), which they related to the falling density (which makes the liquid more “gas-like”). It was common at the time to assign halide-exchange equilibria to covalent molten salts, e.g.,



and derive a degree of ionisation (α) at each temperature to quantify this supposed ion association.^{2,17-22} However, we reported in 2012 the results of *ab initio* molecular dynamics (AIMD) simulations which showed that molten BiCl_3 is a network liquid with very little molecular character, and instead put forward a new theory to explain the conductivity maximum vs temperature.^{23,24} The new theory attributed conductivity to atomic ions “hop[ping] from counterion to counterion,” and used a density-dependent Arrhenius equation to ascribe the maximum to the competing effects of rising hopping opportunities (rising frequency factor A with thermal expansion) and diminishing hopping probability per opportunity (due to rising activation energy E_a as the hopping distance increases with thermal expansion):

$$\sigma(T, \rho) = A(\rho)e^{-E_a(\rho)/RT}. \quad (1)$$

In this paper, we test AIMD simulations and the new conductivity theory on two more molten salts: another high-conducting network liquid (SnCl_2) and a low-conducting molecular liquid (HgBr_2). Despite statistical uncertainty, the AIMD simulations appear to have successfully reproduced the conductivity maximum for both liquids, and thus provide sufficient realism to allow their use in investigating the

^{a)} Author to whom correspondence should be addressed. Electronic mail: allan.east@uregina.ca.

nature of the conductivity maxima. The simulations of HgBr₂ revealed that our hopping mechanism idea is really none other than the Grotthuss conductivity mechanism but for *ions other than H⁺*, a possibility offered by Grotthuss in his original 1805-06 paper.²⁵ The idea was resurrected by Erdey-Grúz in 1937,²⁶ but dismissed by Janz in the 1950s,² and has received little attention since.²⁷ We resurrect and develop the idea once more.

We have implicitly assumed there are no experimental artefacts causing the conductivity falloff at high temperatures. Such possibilities are discussed in the [Appendix](#).

II. METHODS

Simulations were performed as before:²³ the Vienna *Ab initio* Simulation Package (VASP) software^{28,29} was used, with its potpawGGA plane-wave basis sets,^{30,31} standard precision (PREC = NORMAL), ENMAX = 400 eV, isotope-averaged masses, a Nosé thermostat for canonical-ensemble (NVT) conditions³² with 40 fs thermal oscillations (SMASS = 0), and a Verlet velocity algorithm.³³ The Monkhorst-Pack scheme for 10 × 10 × 10 k-point mesh in the Brillouin zone was applied. The time step τ was 4 fs for SnCl₂ but 6 fs for HgBr₂. The cubic simulation cell consisted of 120 atoms (M₄₀X₈₀) and was replicated using periodic boundary conditions to mimic the bulk liquid. All the simulations were done on Dextrose, a supercomputer at the University of Regina, in production runs (“prods”) of 5000 time steps at a time (each run taking several days). Visualization of simulation movies and radial distribution plots were done with VMD software.³⁴ Note that VASP uses plane-wave basis sets that have relativistic effects built in, from a scalar relativistic treatment that initially treated mass-velocity, Darwin, and higher order terms, and lastly included spin-orbit interaction as a perturbation.³⁵

For forces, the PW91 level of density functional theory was used,³⁶ but with an added Grimme-style van-der-Waals (vdW) attractive potential.³⁷ Grimme parameters for mercury were taken to be $C_6 = 42.807 \text{ J nm}^6 \text{ mol}^{-1}$ and $R_0 = 1.6 \text{ \AA}$; the former was calculated by averaging the C_6 values of Tl (computed by using the UPBE0/QZVP recipe Grimme used), the element immediately after Hg, and Xe, the last noble gas before Hg, and the latter was taken to be the same as Grimme used for Cd, the element above it in the periodic table, due to the lanthanide contraction rule.

Both liquids were simulated at six different temperatures. Cell widths were chosen to match orthobaric densities given by Janz:³⁸

$$\rho(\text{SnCl}_2, \text{g ml}^{-1}) = 4.016 - 0.001\,253\,T(K), \quad (2)$$

$$\rho(\text{HgBr}_2, \text{g ml}^{-1}) = 6.7715 - 0.003\,233\,1\,T(K). \quad (3)$$

Starting geometries were arrays of somewhat randomly scattered neutral molecules at a low density. They were equilibrated (~5000 time steps) at a high temperature, and then the final set of Cartesian coordinates was scaled to be a starting geometry for all 6 temperatures (which require different cell volumes). These were then equilibrated for a further 2000 time steps at each temperature, before production-run sampling

began. The number of consecutive 5000-time step production runs at each temperature was 15 for SnCl₂, 16 for HgBr₂ at the three lowest temperatures, and 20 for HgBr₂ at the three highest temperatures.

The simulations generate output of atomic Cartesian coordinates for each time step. From these, the specific conductivity (σ) and atomic diffusion constants (D) were calculated with in-house Fortran programs via Einstein formulae,

$$D_X^{Ein} = \lim_{t \rightarrow \infty} \text{ein}_D(t), \quad \text{ein}_D(t) = \frac{\langle \langle |\vec{r}_{X,i}(t) - \vec{r}_{X,i}(t_0)|^2 \rangle \rangle}{6t}, \quad (4)$$

$$\sigma^{Ein} = \frac{1}{VkT} \lim_{t \rightarrow \infty} \text{ein}_\sigma(t), \quad \text{ein}_\sigma(t) = \frac{\langle |\vec{M}(t) - \vec{M}(t_0)|^2 \rangle}{6t}, \quad (5)$$

where $\vec{r}_{X,i}(t)$ is the Cartesian position of the i th atom of type X at time t , $\vec{M}(t)$ is the total electric dipole of one simulation cell's worth of liquid at time t , V is the volume of the cell, T is temperature in Kelvin, and $\langle \rangle$ denote averaging over all choices of t_0 (Eqs. (4) and (5)) and i (Eq. (4)). The $\vec{M}(t)$ was computed by assigning atomic ions (M²⁺ and X⁻) to all atomic locations regardless of molecularity, and the cell's worth of atoms (120) had to be tracked as they left the original simulation cell, as Hansen³⁹ has done. Einstein formulae appeared to give slightly more precise results than the Green-Kubo method for BiCl₃.²³ For SnCl₂, the “Einstein functions” $\text{ein}(t)$ were obtained from a set of 75 000 time steps of data by averaging 55 000 $\text{ein}(t)$ functions of length 20 000 τ , the functions differing only by choice of time zero (t_0). For HgBr₂, the $\text{ein}_D(t)$ functions were obtained by averaging 60 000 (low T) or 80 000 (high T) such functions of length 20 000 τ , but the $\text{ein}_\sigma(t)$ functions were obtained by averaging shorter functions of length 2000 τ from punctuated time regions (see Sec. III D).

Extrapolation of the Einstein functions to $t \rightarrow \infty$ was done in different ways. In the case of SnCl₂, these functions achieved their asymptotic values quite early, and we did as with BiCl₃:²³ the values of the functions were recorded every 25 τ and were averaged after 1000 τ . The range (max - min) of these plucked values was taken to be the uncertainty s we report on the mean estimate, namely, $\langle x \rangle \pm s$, since traditional estimators of uncertainty could not be used on such heavily serially correlated data. In the case of HgBr₂, the mean and range-based uncertainty for each atomic diffusion constant was obtained from the last 10 000 values of the respective Einstein function. However, for HgBr₂ conductivity, the $\text{ein}_\sigma(t)$ exhibited continual slow decay of the form in Eq. (6),

$$\text{ein}_\sigma(t) \approx a + \frac{b}{t} + \frac{c}{t^2}, \quad (6)$$

$$\sigma = \frac{1}{VkT} \lim_{t \rightarrow \infty} \text{ein}_\sigma(t) = \frac{a}{VkT}. \quad (7)$$

For reproducibility reasons, instead of determining a by performing least-squares fitting of Eq. (6), it was much more reliable to perform linear least-squares fitting of $t \cdot \text{ein}_\sigma(t)$ vs t via Eq. (9),

$$t \cdot \text{ein}_\sigma(t) \approx at + b + \frac{c}{t}, \quad (8)$$

$$t \cdot \text{ein}_\sigma(t) \approx at + b \text{ at large } t \quad (9)$$

and its slope is then the a used to compute $\sigma = a/VkT$. To perform linear regression, it was necessary to choose a valid data range, i.e., to choose the time step of the onset of a constant asymptotic slope. This was not easy to do. Hence, at each of the 6 temperatures, we obtained 6 estimates of the slope of $t\text{-}e_{\text{in}}(t)$ by varying the asymptote onset to be $t = 400, 500, 600, 700, 800,$ or 900 time steps and taking the slope of the function from here to its end at time step 2000. The mean and standard deviation of these 6 estimates were taken and converted to conductivity and uncertainty values by multiplying by $1/VkT$. The uncertainty due to choice of asymptote onset was deemed to be larger than other statistical uncertainties in these particular predictions, except perhaps an uncertainty in taking a regression over a small (<2000 step) time window; this latter uncertainty of unknown magnitude would cause larger net uncertainties.

Ion analysis for the HgBr_2 simulations was also done using in-house Fortran programs developed for this particular liquid. One of them (*ionsdetect.exe*) reports for each time step and each Hg atom the size of the molecule or molecular ion it is in, using a bond cutoff criterion of 2.8 \AA chosen to match the location of the minimum in radial distribution plots generated from the simulations. The sizes were assumed to correspond to either neutral or singly charged species, i.e., $\text{Hg}_n\text{Br}_{2n}$, $\text{Hg}_n\text{Br}_{2n-1}^+$, or $\text{Hg}_n\text{Br}_{2n+1}^-$ only. (The number of loose Br^- ions, omitted by *ionsdetect.exe*, was found by counterbalancing the total anions to the total cations.) Note that if an ion had, e.g., three Hg atoms at some instant, the size of that species was printed thrice by the program; correcting for this overcounting was straightforward. These lists of species sizes were used to count species “hits” and converted to average concentrations for each 10 000- time step data set, and the means and standard deviations of concentrations across data sets are reported. The second program (*ionlife.exe*) reports the average lifetime of an HgBr^+ ion, using the output of *ionsdetect.exe*: it adds the total number of times a 2 occurs (as HgBr^+ is diatomic) and then divides this sum by the number of times such an ion disappears (number of lifespans). These average lifetimes were computed for each 10 000- time step data set, and the means and standard deviations of these individual data set values are reported.

The very few geometry optimizations that were performed were done using Gaussian 09 software on Dextrose, at the PW91/SDD level of theory.⁴⁰

III. RESULTS

A. SnCl_2 liquid structure

SnCl_2 exists in the gas phase as bent monomer molecules ($\sim 1\%$ dimers).⁴¹ The solid phase exists as polymeric chains of $-\text{Sn}(\text{Br})-\text{Br}-\text{Sn}(\text{Br})-\text{Br}$ -type, with Sn having a tight coordination number of 3 (bond lengths of $\text{Sn}-\text{Cl}_{\text{terminal}} = 2.66 \text{ \AA}$ and $\text{Sn}-\text{Cl}_{\text{bridging}} = 2.78 \text{ \AA}$) and a loose coordination number of 7 (the next four Cl being $3.0\text{-}3.3 \text{ \AA}$ away).⁴² It has a molten range of $247\text{-}650 \text{ }^\circ\text{C}$.⁴³ The orthobaric specific-conductivity maximum is at $873 \pm 3 \text{ }^\circ\text{C}$.^{14,43}

From the simulation movies ($560\text{-}960 \text{ }^\circ\text{C}$), the structure of molten SnCl_2 is that of a *network covalent liquid*, quite

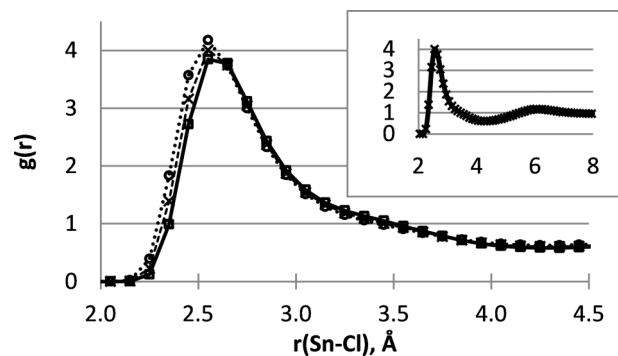


FIG. 1. Radial distribution plots for SnCl_2 from AIMD simulations. Squares: $640 \text{ }^\circ\text{C}$. X's (including inset): $800 \text{ }^\circ\text{C}$. Circles: $960 \text{ }^\circ\text{C}$.

similar to that of BiCl_3 : the simulated liquid consisted of highly mobile Sn^{2+} and Cl^- ions, with no definite ionic or covalent molecular structures seen. Chloride ions were either bridged between two Sn^{2+} ions or bonded to a single Sn^{2+} at any given instant, but frequently hopped between Sn^{2+} partners and were quite mobile, on very short time scales. Polymeric chains, as concluded by Clarke and Solomons from lower-temperature Raman spectra,⁴⁴ were not observed.

Radial distributions of Cl from Sn, generated from the simulations, are shown in Fig. 1 and reveal a larger peak at 2.6 \AA for singly coordinate Cl and a broader shoulder centred perhaps at 3.4 \AA for bridging Cl. The computed “loose” (N) and “tight” (TN) coordination numbers from the integration of the $g(r)$ functions are listed in Table I. In comparing the chloride coordination numbers of SnCl_2 here to those of BiCl_3 ,²³ $\text{TN}_{\text{Cl}} \approx 1$ in both liquids but in SnCl_2 $N_{\text{Cl}} \approx 3$, while in BiCl_3 $N_{\text{Cl}} \approx 2$,²³ the difference is likely due to both cations (Bi^{3+} and Sn^{2+}) preferring to be 6-coordinate in the melts.

B. SnCl_2 conductivity and diffusion

Table II reports the computed diffusion coefficients D_{Cl} and D_{Sn} (Eq. (4)) and specific conductivities σ (Eq. (5)). Despite statistical errors due to finite sampling, the predicted conductivities produced a maximum at $880 \text{ }^\circ\text{C}$ in agreement with experiment. All the computed σ values are slightly high, within a factor of 2 of the experimental data. More sampling was needed to see this maximum for SnCl_2 than was needed for BiCl_3 ,²³ for unknown reasons. The computed

TABLE I. Coordination (N) and tight coordination (TN) numbers computed from $g(r)$ plots generated by VMD. Cutoffs were 4.1 \AA for N and 2.8 \AA for TN, each 0.1 \AA larger than those used for BiCl_3 (Ref. 23).

T ($^\circ\text{C}$)	ρ (g/ml)	N_{Sn}	N_{Cl}	TN_{Sn}	TN_{Cl}
560	2.9721	6.299	3.149	2.259	1.129
640	2.8718	6.096	3.048	2.236	1.118
720	2.7716	5.901	2.950	2.220	1.110
800	2.6713	5.721	2.861	2.201	1.101
880	2.5711	5.538	2.769	2.180	1.090
960	2.4709	5.378	2.689	2.164	1.082

TABLE II. Specific conductivity σ and diffusion coefficients D for SnCl_2 from present simulations. The σ^{expt} values are from fitting to Ref. 14 data. Uncertainties in parentheses.

T (°C)	ρ (g/ml)	σ^{Ein} ($\Omega^{-1} \text{cm}^{-1}$)	σ^{expt} ($\Omega^{-1} \text{cm}^{-1}$)	$D_{\text{Sn}}^{\text{Ein}}$ ($10^{-9} \text{m}^2 \text{s}^{-1}$)	$D_{\text{Cl}}^{\text{Ein}}$ ($10^{-9} \text{m}^2 \text{s}^{-1}$)
560	2.9721	2.4(1.4)	2.33	3.4(0.3)	5.1(0.3)
640	2.8718	3.0(0.6)	2.54	5.0(0.2)	6.7(0.4)
720	2.7716	3.3(0.5)	2.70	5.8(0.2)	8.8(0.1)
800	2.6713	3.8(0.4)	2.77	7.6(0.7)	10.5(0.2)
880	2.5711	4.4(1.5)	2.82	10.3(1.6)	13.2(0.3)
960	2.4709	2.5(0.7)	2.77	12.0(1.7)	16.0(0.7)

diffusion coefficients steadily increase with temperature, with Cl diffusing faster than Sn at all temperatures, and the gap is bigger at higher temperatures, trends identical to those seen with BiCl_3 .

The Einstein functions used in the calculations of σ and the diffusion constants appear in Fig. 2. The $\text{ein}_\sigma(t)$ function

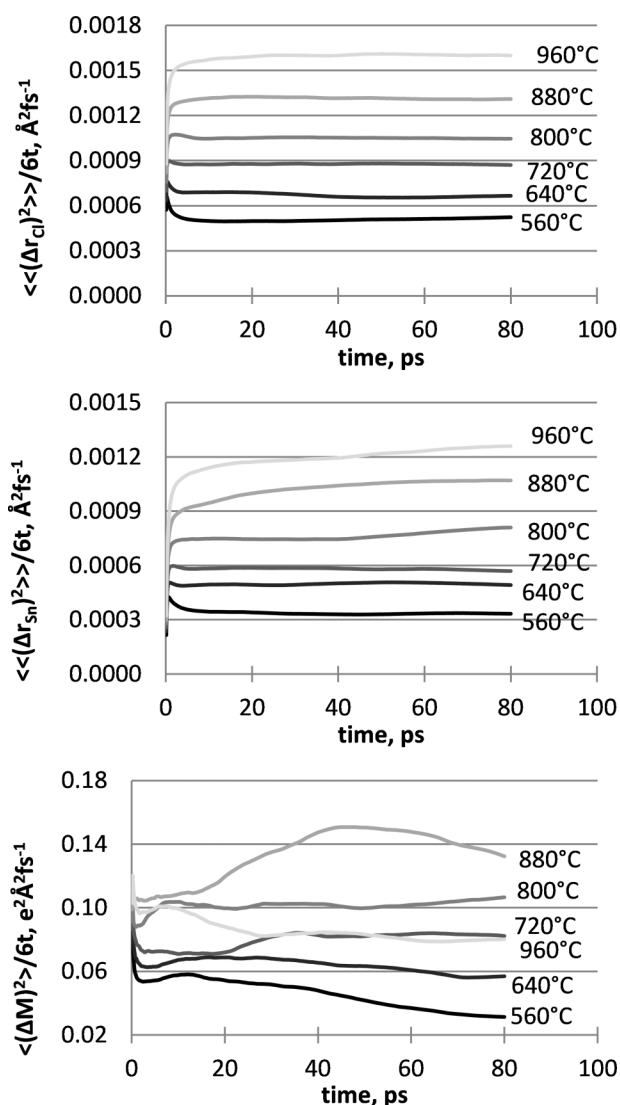


FIG. 2. The Einstein diffusion and conductivity functions for molten SnCl_2 from present simulations.

shows the same “wandering” nature observed for BiCl_3 , while the $\text{ein}_D(t)$ functions are much better behaved.

C. HgBr_2 liquid structure

It is known that HgBr_2 exists as linear triatomic molecules in all phases, with solid-state intra- and inter-molecular Hg–Br distances of 2.5 and 3.2 Å.¹⁸ It has a molten range of 238–319 °C.¹⁸ HgBr_2 exhibits a strong Raman symmetric Br–Hg–Br stretch band in all phases (184, 195, 225 cm^{-1} in solid, liquid, gas, respectively),^{19,20} the similarity of the value in the solid and molten phases shows that some of the intermolecular forces (multipole dispersion type) from the solid state are retained in the liquid state. We have not found any reports of spectroscopic detection of ions in the melt.

From the simulation movies, the structure of molten HgBr_2 is confirmed to be that of a molecular liquid, unlike the network covalent liquids SnCl_2 and BiCl_3 . Interestingly, the movies of molten HgBr_2 also reveal frequent metathesis-like concerted bromine exchanges between molecules (Fig. 3). On the potential energy surface (PES), the dimer is weakly bound (5.5 kcal mol^{-1} , PW91/SDD), but at the temperatures of concern there is likely to be no bound dimer on the free energy surface (FES), since the simulations show no vibrating dimers as intermediates. The frequency of metathesis attempts (not all were successful) was 50 per cell per 1000 time steps at 680 °C, i.e., each HgBr_2 molecule experiences one every 5 ps.

Radial distributions of Br from Hg, generated from the simulations, are shown in Fig. 4 and reveal a clear separation of the large peak for singly coordinate halide (2.5 Å) from a broader peak at 3.4 Å for four non-covalent Hg–Br distances around each Hg atom, slightly expanded from 3.2 Å in the solid state.¹⁸

In lieu of the coordination number analysis we used on the network liquids BiCl_3 and SnCl_2 , for this molecular liquid we determined species identities and concentrations, and HgBr^+ ion lifetimes, using FORTRAN programs (see Methods). Concentrations are reported in Table III. As temperature increases, the monomer concentration $[\text{HgBr}_2]$ falls, the dimer concentration $[\text{Hg}_2\text{Br}_4]$ goes through a maximum, and all ion concentrations increase.

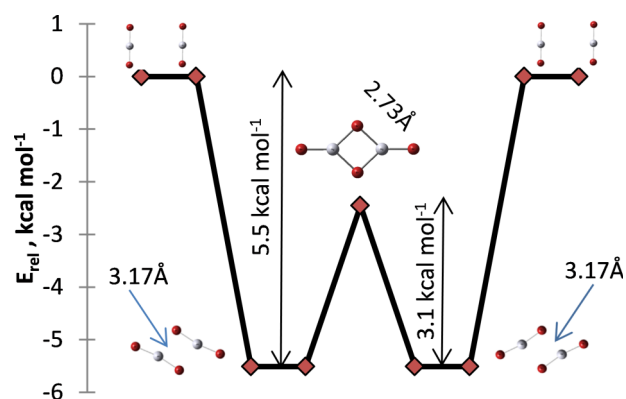


FIG. 3. The potential energy surface for HgBr_2 metathesis (PW91/SDD).

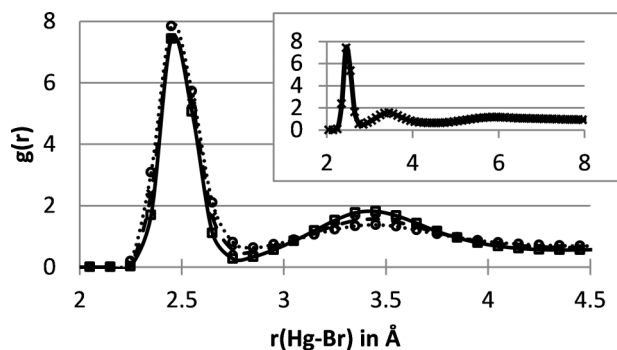
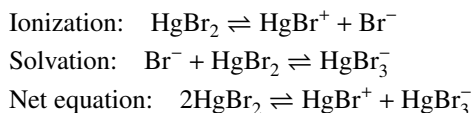


FIG. 4. Hg–Br radial distribution in molten HgBr_2 at different temperatures. Squares: 280 °C. X's (including inset): 440 °C. Circles: 600 °C. From non-hyperactive simulation data sets only (see Sec. III D).

This last aspect is particularly important, as it contradicts long-standing claims of ion association in mercuric halides at high T. For example, the ion association was thought by Janz^{18–20} to be a shift to the left in equilibrium of



While such equilibria (and others involving larger oligomers) exist in the simulated liquid, the shift to the left at high T did not. To further stress the problems with classical ion-association assumptions, we also computed the degree of ionization $\alpha(T)$ directly from our ion concentrations reported in Table III, obtaining values of 0.007 (280 °C) to 0.055 (680 °C). These are 100 times larger than the poor estimate (0.0002) made by Janz^{19,20} who assumed that all deviations from Walden's Rule (which works well for the fully ionized molten alkali halides) were due to ion association. Thus, the conductivity maximum versus T that arises from our simulations did *not* arise from increased ion association (a drop in α).

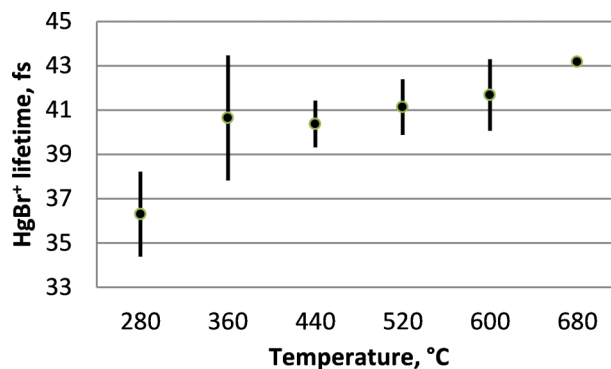


FIG. 5. Average lifetime of an HgBr^+ ion vs temperature from the simulations. From non-hyperactive simulation data sets only (see Sec. III D).

The apparent error made by Grantham and Yosim,^{13–16} Janz,^{2,18–20} Tödheide,^{21,22} and others was in assuming the mode of conduction is classical translation of molecular ions, when instead it is via the Grotthuss mechanism. In the simulations, the decline in HgBr_2 conductivity past the maximum is due to a drop in ion mobility, not ion concentration. Another result regarding liquid structure that is relevant in this regard is the plot of ion lifetime versus temperature (Fig. 5): note first the very short lifetimes (36–43 fs) but also the rise in lifetime with temperature which is offered as evidence of a retardation of the Grotthuss rate (and hence of conductivity).

D. HgBr_2 : Grotthuss mechanism observation and “lock” problem

The Grotthuss “hopping” mechanism for conductivity was observed in simulations of HgBr_2 artificially seeded with molecular ions. Two such simulations (at 680 °C and 280 °C, respectively) were run starting with 38 HgBr_2 , one HgBr^+ , and one HgBr_3^- . Ion neutralisation occurred via Grotthuss mechanism in both runs: after 375 time steps and 5 Br^-

TABLE III. “Instantaneous” species concentrations in molten HgBr_2 from non-hyperactive simulation data sets only (see Sec. III D). Uncertainties in parentheses. Species larger than 12 atoms are present in $<0.001 \text{ mol l}^{-1}$ concentrations. Note that ion lifetimes are extremely small (~ 10 fs, see Fig. 5).

# Atoms	Species	Species concentrations (in mol l^{-1}) at different temperatures					
		280 °C	360 °C	440 °C	520 °C	600 °C	680 °C
1	Br^-	0.04(1)	0.08(2)	0.11(1)	0.15(3)	0.18(2)	0.21(1)
2	HgBr^+	0.03(1)	0.06(1)	0.09(1)	0.12(2)	0.15(2)	0.18(1)
3	HgBr_2	13.0(1)	12.0(1)	11.1(1)	10.3(1)	9.6(1)	8.80(4)
4	HgBr_3^-	0.009(3)	0.021(4)	0.029(5)	0.04(1)	0.05(1)	0.058(3)
5	Hg_2Br_3^+	0.020(6)	0.04(1)	0.045(8)	0.06(1)	0.07(1)	0.08(1)
6	Hg_2Br_4	0.33(3)	0.40(2)	0.42(2)	0.42(2)	0.41(1)	0.382(1)
7	Hg_2Br_5^-	0.001(1)	0.004(1)	0.004(2)	0.007(3)	0.008(2)	0.011(1)
8	Hg_3Br_5^+	0.003(2)	0.008(2)	0.010(3)	0.012(3)	0.016(4)	0.018(3)
9	Hg_3Br_6	0.024(6)	0.037(5)	0.041(2)	0.045(7)	0.044(5)	0.047(2)
10	Hg_3Br_7^-	0.000(0)	0.001(1)	0.001(1)	0.001(1)	0.002(1)	0.002(1)
11	Hg_4Br_7^+	0.001(1)	0.002(1)	0.002(1)	0.002(1)	0.003(1)	0.003(1)
12	Hg_4Br_8	0.003(1)	0.005(2)	0.005(1)	0.006(2)	0.006(2)	0.006(1)
Total ions		0.10(2)	0.20(4)	0.30(4)	0.40(8)	0.47(6)	0.56(3)

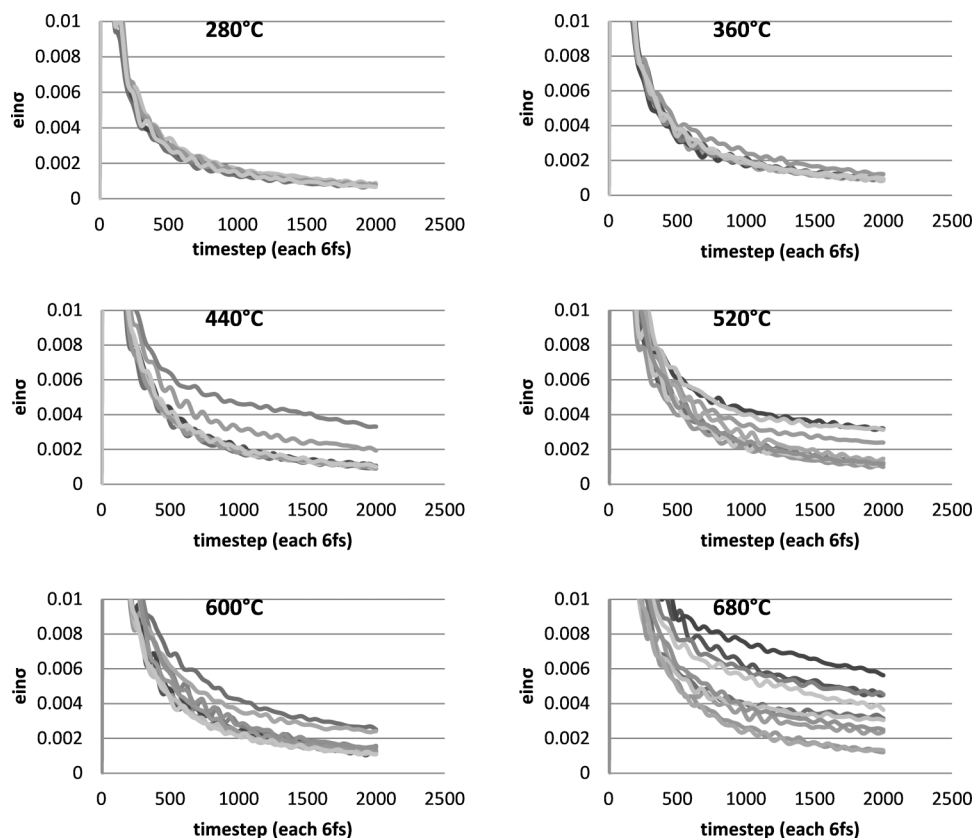


FIG. 6. The $\text{ein}_\sigma(t)$ curves ($n_{\text{inf}} = 2000$, $n_{\text{zero}} = 8000$) for different 10 000-time step data sets (time segments) of HgBr_2 simulations, at six different temperatures. Conductivity is proportional to $t \rightarrow \infty$ asymptotes.

transfers at 680°C , and after 385 time steps and 4 Br^- transfers at 280°C . The transfers originated from HgBr_3^- . Thus, HgBr_2 , like H_2O , can be said to conduct electricity via Grotthuss mechanism. We propose using the Grotthuss label

for the “hopping” mechanism we proposed for the network covalent salts as well (BiCl_3 and SnCl_2), where the hopping is more subtle and particular “relays” cannot be easily identified in the simulations.

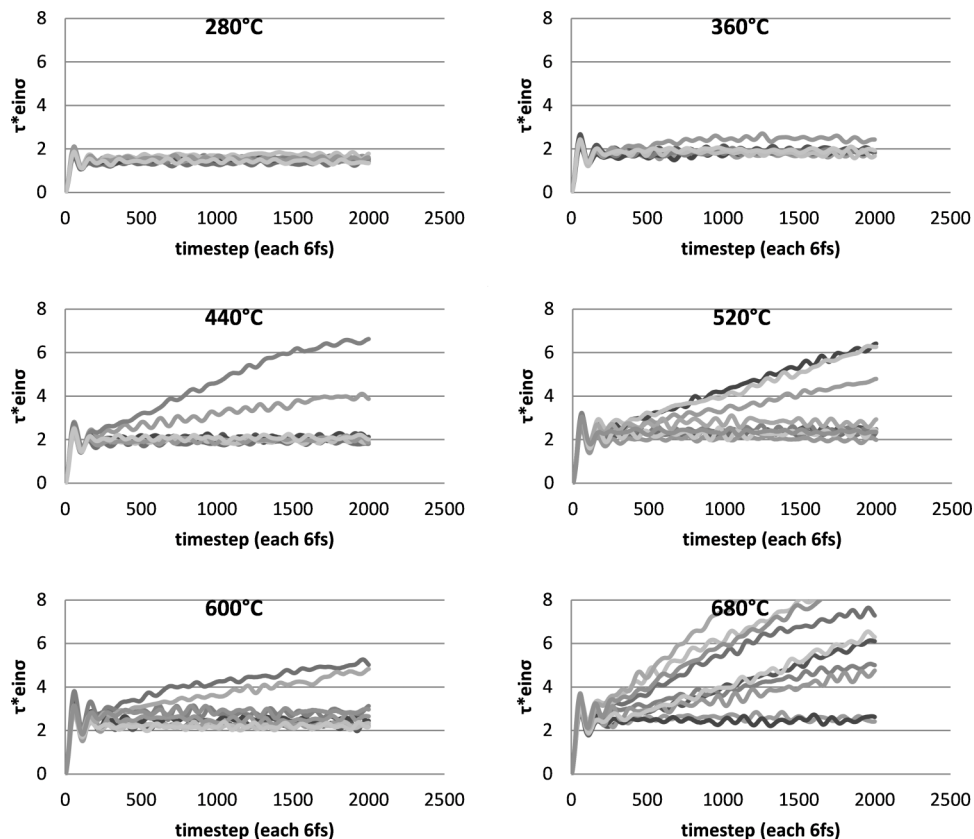


FIG. 7. The $t \cdot \text{ein}_\sigma(t)$ vs t plots (t in units of time step) for different 10 000-time step data sets (time segments) of HgBr_2 simulations, at six different temperatures. Conductivity is proportional to the slopes of these curves.

We also report here, as a caution to others, a conductivity simulation problem we encountered with HgBr_2 which we shall term the Grotthuss “lock” problem. When we first computed the conductivities from the HgBr_2 simulations, the conductivities were overpredicted by 1-2 orders of magnitude. To investigate why, specific conductivities were calculated for each 10 000- time step data set (two consecutive production runs) for all the temperatures. Fig. 6 shows $\text{ein}_o(t)$ curves at each temperature and Fig. 7 shows the corresponding $t\text{-ein}_o(t)$ vs t plots, where t is in units of 6 fs.

In Figs. 6 and 7, one sees a minority of “hyperactive” data sets (0, 1, 2, 3, 2, 8 at the 6 temperatures from 280 to 680 °C) whose curves disagree with the majority of curves, extrapolating too high in Fig. 6 and having overly large slopes in Fig. 7. These hyperactive curves produce overly high conductivity values, while the non-hyperactive curves produce reasonable predictions. Hence, focus was turned to investigating the reasons for overconductivity in the hyperactive data sets.

Plots of net dipole moment drift squared (the numerator in the $\text{ein}_o(t)$ expression given in Eq. (5)) versus time step revealed singular instances of large jumps over very small time windows. Careful analysis of the molecular movie for one such small time window (in run “prod09” of 440 °C) revealed an artefact due to the limited cell size (17-18 Å): a Grotthuss relay of bromide ions which began at one Hg atom, extended to a neighbouring replicant cell, and finished at the replicate of the same Hg from which the relay started. Its details are given in Fig. 8. The relay started with a dimerization of two HgBr_2 molecules at $\tau = 1204$ which then ionized to an Hg_2Br_3^+ and a Br^- at $\tau = 1232$. The Br^- remained solvated between three neutral HgBr_2 molecules for roughly 80 time steps before bonding to a neutral HgBr_2 molecule at $\tau = 1310$, initiating a Br^- transfer relay. The relay ended when finally a Br^- finds a replicant of the original cation (Hg_2Br_3^+) in a replicant cell, which at time of arrival ($\tau = 1508$) had already parted as HgBr^+ and HgBr_2 .

This Grotthuss relay correlated in time with the only jump in the dipole moment drift in the run “prod09,” and hence caused the high conductivity prediction. We refer to

TABLE IV. Specific conductivity σ and diffusion coefficients D for HgBr_2 from present simulations. The σ^{expt} values are from fitting to Ref. 14 data. σ^{Ein} calculated from non-hyperactive simulation data sets only; D^{Ein} calculated from all data sets.

T (°C)	ρ (g/ml)	σ^{Ein} ($\Omega^{-1} \text{cm}^{-1}$)	σ^{expt} ($\Omega^{-1} \text{cm}^{-1}$)	$D_{\text{Hg}}^{\text{Ein}}$ ($10^{-9} \text{m}^2 \text{s}^{-1}$)	$D_{\text{Br}}^{\text{Ein}}$ ($10^{-9} \text{m}^2 \text{s}^{-1}$)
280	4.9833	0.0010(5)	0.000 22	0.9(0)	1.0(0)
360	4.7246	0.0011(6)	0.000 35	1.6(0)	1.8(2)
440	4.4660	0.0021(4)	0.000 40	2.4(1)	2.7(1)
520	4.2073	0.0007(2)	0.000 36	4.0(1)	4.1(1)
600	3.9487	0.0006(4)	0.000 24	5.6(0)	6.0(1)
680	3.6900	-0.0004(2)	0.000 04	7.4(1)	7.7(1)

this artefact as a “lock” because the net result is a shift in the centre of mass of all Hg atoms in one direction and in the centre of mass of all Br atoms in the opposite direction, causing the rise in the net dipole moment drift which locks into a higher value. Such a lock is artificial (due to the periodic replication of the simulation cell). It is very likely that all the hyperactivity seen in Figs. 6 and 7 are due to such artificial locks.

Therefore, the $t\text{-ein}_o(t)$ functions from all the hyperactive data sets were dismissed for being defective, and the remaining $t\text{-ein}_o(t)$ functions in Fig. 7 were averaged (at each temperature) for final $t\text{-ein}_o(t)$ functions at each temperature. These grand-averaged curves had their slopes extrapolated to infinity to obtain the specific conductivities (Sec. III E).

E. HgBr_2 conductivity and diffusion

Table IV reports the computed diffusion coefficients D_{Cl} and D_{Sn} (Eq. (4)) and specific conductivities σ (Eq. (5)); the calculation for σ involved only non-hyperactive data sets. Again, as for the higher-conducting network liquids BiCl_3 and SnCl_2 , the simulations of this molecular liquid qualitatively reproduced the conductivity maximum. This was a pleasant surprise, given the much smaller conductivities of HgBr_2 vs BiCl_3 and SnCl_2 (factor of 1000, see Table II) which required significant reduction of absolute error. The

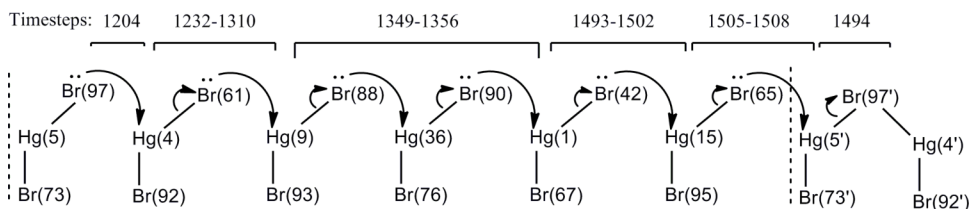
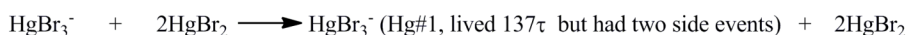


FIG. 8. The Grotthuss relay in prod09 of 440 °C which coils to the starting point in a replicant cell, leading to a jump in the net dipole moment drift and the overprediction of conductivity.



predicted conductivities are factors of 2-5 too high (except at 680 °C), possibly due to the approximate DFT forces, but the prediction at 440 °C is particularly poor and overly precise due to an unfortunate, random, upwards wandering of the averaged $\text{t.ein}(t)$ curve at the end of our sampling range, which made all six slope (and hence conductivity) predictions too large at that temperature.

In contrast to conductivity, there was no evidence of hyperactive atomic diffusion. Diffusion constants of Hg and the much lighter Br are nearly identical, which is logical since they generally translate together in triatomic molecules.

IV. DISCUSSION

With the observation in simulation of a Grotthuss relay of Br^- ions in the molecular liquid HgBr_2 , we now suggest that the “hopping” ideas we proposed earlier^{23,24} be recast as density-dependent aspects of a general Grotthuss conductivity mechanism for all ions. A comparison with previous literature discussion of the Grotthuss mechanism of H^+ in aqueous media is then apt. The goal of this discussion is to understand the conductivity maxima with temperature observed experimentally by Grantham and Yosim¹³⁻¹⁵ and in simulations by us for SnCl_2 (here), HgBr_2 (here), and BiCl_3 (previously²³).

Let us first recap basic equations for conductivity. If an external electric field of magnitude X (units: V cm^{-1}) induces a steady current density i (units: $\text{C cm}^{-2} \text{s}^{-1}$) in a material, the specific conductivity σ of the material is the proportionality constant: $\sigma = i/X$ (units: $\text{C V}^{-1} \text{s}^{-1} \text{cm}^{-1} = \Omega^{-1} \text{cm}^{-1}$).⁴⁵ The current density i is the total charge flowing through an area perpendicular to the external field, per unit time; an equation for i is

$$i = \sum_j q_j \rho_j v_j, \quad (10)$$

where the sum is over ion types j , q_j is the charge per ion (units: C ion^{-1}), ρ_j is the ion density (ions cm^{-3}), and v_j is the steady ion drift velocity caused by the external field (cm s^{-1}). The sum includes all charged particles passing through the perpendicular area, e.g., cations in one direction (q and v positive) and anions in the opposite direction (q and v negative). With this equation, σ becomes

$$\sigma = \sum_j q_j \rho_j \mu_j, \quad (11)$$

where $\mu_j = v_j/X$ (units: $\text{cm}^2 \text{V}^{-1} \text{s}^{-1}$) is the “conventional” ion mobility⁴⁵ induced by the external field. (A related quantity sometimes discussed is molar conductivity Λ (units: $\Omega^{-1} \text{cm}^2 \text{mol}^{-1}$) which is defined as $\Lambda = (1000/c_j)\sigma = (1000 N/\rho_j)\sigma$ where c is molarity (units: mol dm^{-3}), N is Avogadro’s number, and the factor 1000 converts cm^3 to dm^3 for cancellation.

It has been a long-standing belief that conductivity maxima could be explained by ion association: in Eq. (11), a fall in ρ_j as μ_j continues to increase with temperature. Since our simulations do not show a loss of free ions at high T and instead Grotthuss-like hopping of atomic ions, we are led to believe that the maxima are due to a high-temperature fall in μ_j (not ρ_j), where j is an *atomic* ion, not a molecular one.

We now discuss effects of a Grotthuss mechanism upon conductivity. First, consider the 1909 data of Johnston⁴⁶ who determined limiting molar conductivities Λ_0 (i.e., in the limit of infinite dilution) for several aqueous salt solutions at several temperatures. At 18 °C, the values ($\Omega^{-1} \text{cm}^2 \text{mol}^{-1}$) were generally 109-131 (KCl, KNO_3 , NaCl, NH_4Cl , and AgNO_3) but were 216 for NaOH solution and 377-379 for solutions of HCl and HNO_3 . The anomalously high conductivity and mobility of OH^- and H_3O^+ ions in water was of substantial interest in the early 20th century, and consensus grew that the excess was due to the Grotthuss mechanism for H^+ in water. These high conductivities are equivalent to *classical* (i.e., non-Grotthuss) conductance of ions of “unreasonably small” sizes ($r_{\text{H}^+} \approx 0.2 \text{ \AA}$, $r_{\text{OH}^-} \approx 0.4 \text{ \AA}$).⁴⁷

Of particular importance here is Johnston’s observed temperature dependence of these aqueous solution conductivities: the pH-neutral salts gave linear plots of σ_0 vs. T, but the acids gave negative curvature (Fig. 9 left). Two questions are here posed and answered. (i) How (if at all) is the Grotthuss mechanism causing the curvatures in $\sigma_{0,\text{HNO}_3}(\text{T})$ vs $\sigma_{0,\text{KNO}_3}(\text{T})$ to be different? (ii) Could this same reason be causing the conductivity maximum in molten salt?

Perusal of textbooks led us to two particular theories of Grotthuss effects. Geirer and Wirtz⁴⁸ dealt with the anomalous Grotthuss conductivity of OH^- and H^+ by assuming, in addition to classical H_3O^+ conductivity, a traditional Arrhenius relation for H^+ mobility

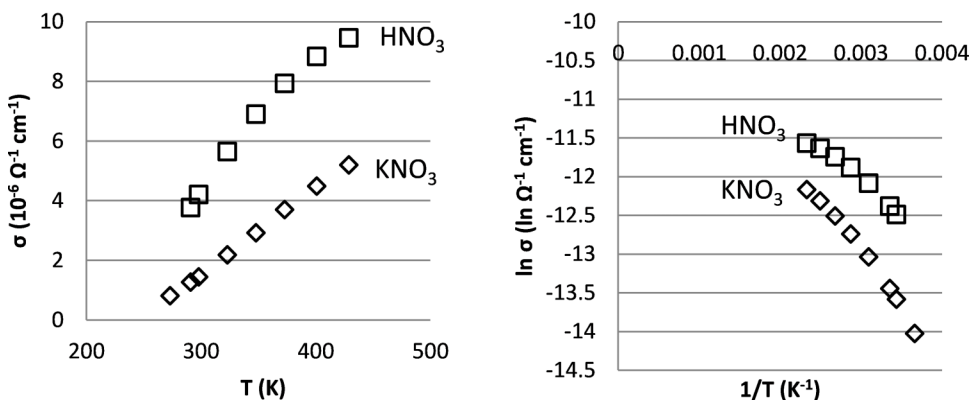


FIG. 9. Specific conductivities vs. temperature (left) and corresponding Arrhenius plots (right) of two aqueous solutions, in the limit of infinite dilution. Data calculated from limiting molar conductivities of Johnston 1909.⁴⁵

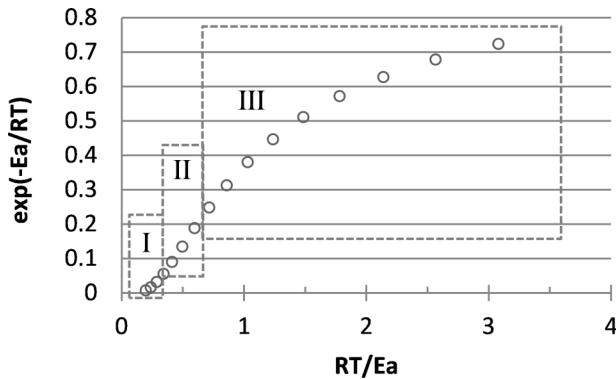


FIG. 10. The three curvature regions of a strict Arrhenius relation: I ($RT/E_a < 1/2$), II ($RT/E_a \approx 1/2$), III ($RT/E_a > 1/2$).

$$\mu = Ae^{-E_a/RT} \quad (12)$$

but imagining in the prefactor A a T -dependent factor for the probability of appropriate H-bond alignment. They assumed this probability decreases with T past $\sim 50^\circ\text{C}$, impeding H^+ mobility. In a more detailed theory, Conway, Bockris, and Linton⁴⁹ viewed Grotthuss conductivity as a sequence of proton-transfer and water-reorientation steps and determined that in this model, the water reorientation step would be rate-determining. They did not write out an expression for net mobility or its temperature dependence, however, and hence is not of help here.

The negative curvature for $\sigma_{0,\text{HNO}_3}(T)$ in Fig. 9 might be due to a falling prefactor A as Geirer and Wirtz hypothesized. Or, it might be due to a rising E_a as the solution expands with rising T , as we proposed for BiCl_3 due to a “hopping” (now termed Grotthuss) mechanism. However, we instead question the need for a special treatment for aqueous acids/bases vis-à-vis aqueous salts, for two reasons. First, *all* aqueous

cases show non-Arrhenius behaviour (see right-hand plot of Fig. 9); Erdely-Grúz comments on the non-constant nature of E_a vs. T for several aqueous solutions.⁴⁷ Second, the curvature change can be linked to a simple change in magnitude of the activation energy, and we shall explain this. Suppose the specific conductivities of the two solutions in Fig. 9 were “strictly” Arrhenius (constant barrier E_a and prefactor A). The derived E_a values from slopes of the Arrhenius plots would then be 2.7 and 1.7 kcal mol⁻¹ for KNO_3 and HNO_3 , respectively. Now, note that strict Arrhenius behaviour of $f(T) = Ae^{-E_a/RT}$ has 3 distinct regions in the $f(T)$ vs. T plot (positive/linear/negative curvature if RT/E_a is $</=> 0.5$, see Fig. 10). The derived E_a values (2.7, 1.7) result in RT/E_a values (0.20-0.30, 0.35-0.45) that sit in two different regions: Region I for aqueous salt, but Region II for aqueous acid. A non-Arrhenius effect adds some negative curvature to both cases, moving the curvature in $\sigma_{0,\text{HNO}_3}(T)$ from linear to negative, and in $\sigma_{0,\text{KNO}_3}(T)$ from positive to linear. Thus, to answer the two posed questions: (i) *in dilute aqueous cases, the Grotthuss nature of H^+ conductivity adds negative curvature to $\sigma(T)$ merely by providing a low activation barrier* and (ii) *this is not the reason for the conductivity maximum in molten salt, since a mere lowering of a constant E_a cannot produce a conductivity maximum* (Fig. 10).

We now turn from aqueous salt to molten salt. Consider the 1947 paper of Bloom and Heymann⁵⁰ who found good Arrhenius behaviour in molten ionic halides (e.g., MgCl_2) but not in “covalent” halides (e.g., PbCl_2) and attributed it to the more covalent character of the bonds involved. Fig. 11 shows exemplary data for 4 molten halides of MX_2 stoichiometry, including the two maxima-producing cases we studied via simulation in this work. From Fig. 11 alone one sees three classes of molten halides. The ionic halide MgCl_2 has, as is typical of the alkali/alkali earth halides, a significantly higher melting point (987 K⁵¹) than the post-transition-metal

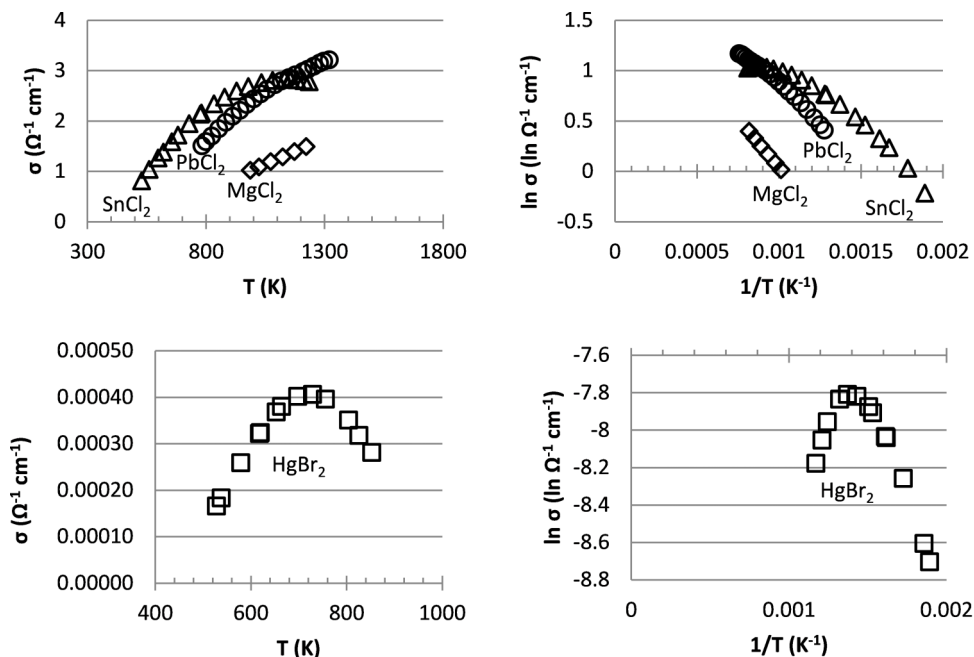


FIG. 11. Specific conductivities vs. temperature (left) and corresponding Arrhenius plots (right) of different molten halides. The increase in covalency is reflected in the increase in negative curvature of the plots in the series Mg, Pb, Sn, Hg. Data from Refs. 14, 52 (MgCl_2), and 53 (PbCl_2).

halides, which we sub-classify as network covalent halides (PbCl_2 774 K,⁵¹ SnCl_2 520 K⁴³) or molecular covalent halides (HgBr_2 511 K¹⁸). Note that the two network covalent halides have twice the conductivity as the ionic halide at a common temperature (upper left plot of Fig. 11), but the molecular covalent halide has orders of magnitude less conductivity (bottom right plot of Fig. 11). We pose, for molten salt, the main question just posed for dilute aqueous solutions: How (if at all) is the Grotthuss mechanism causing the curvatures in $\sigma_{\text{ionic}}(T)$ vs $\sigma_{\text{covalent}}(T)$ to be different, so much so that maxima are created?

Angell⁵⁴ offered a justification for the use of a modified Arrhenius equation in which T is replaced by $T-T_0$ (e.g., the Vogel-Fulcher-Tammann or VFT equation⁵⁵), with T_0 being the temperature at which conductivity drops to zero due to formation of glass (hypothetically in the case of pure molten salts). Invoking T_0 is useful for modelling conductivity at very low liquid temperatures,^{54,55} close to T_0 , for example, (i) molten salt mixtures, which have suppressed crystallization points, (ii) supercooled pure molten salts, and (iii) pure ionic liquids with large alkylated cations resistant to crystallization. Invoking T_0 perhaps becomes less important as T increases away from T_0 . Most importantly, the mere incorporation of T_0 into a strict Arrhenius equation cannot account for a conductivity maximum. Some other effect in the covalent halide cases is apparent.

Okada and Takagi,⁵⁶ in analyzing the conductivity maximum of molten TlCl with classical molecular dynamics simulations, assumed that the maximum in $\sigma(T)$ was due to the drop in density outpacing the rise in Arrhenius mobility (see Eq. (11)). However, if this were the case, then molar conductivity $\Lambda(T)$ would have no maximum. Maxima in $\Lambda(T)$

can be easily demonstrated for several systems by dividing known $\sigma(T)$ data by known $\rho(T)$ data. Some other effect is still apparent.

We first address the network covalent cases (PbCl_2 and SnCl_2). Since the ionic halides (e.g., MgCl_2), with minimal Grotthuss effects, show good Arrhenius behaviour (up to 1200 K at least), let us assume they are of strict Arrhenius nature; for MgCl_2 this produces $A = 7.3 \Omega^{-1} \text{cm}^{-1}$ and $E_a = 3.88 \text{ kcal mol}^{-1}$. PbCl_2 and SnCl_2 conduct more than twice as well as MgCl_2 at 990 K, despite lower molar concentrations at this temperature ($[\text{Mg}]$, $[\text{Pb}]$, $[\text{Sn}]$ would be 17.7, 16.6, 14.6 M, respectively, at 990 K using Janz density equations;³⁸ chloride concentrations are double these amounts by stoichiometry), and thus at first glance, the conjecture used for aqueous-acid $\sigma(T)$ curvature might apply here as well: a lowered E_a for network covalent melts (which would explain the higher conductivity) might move us from Region II to Region III in Fig. 10, imparting negative curvature. However, as already mentioned, this lowering of E_a within a strict Arrhenius relation cannot account for a conductivity maximum. Some further effect is still apparent. Since the maximum occurs while the halide is still essentially 3-coordinate, we are still in favour of applying our BiCl_3 argument here to SnCl_2 : in *network covalent molten halides, the Grotthuss nature of halide conductivity adds negative curvature to $\sigma(T)$ by providing a rising E_a during thermal expansion* which outpaces the rise in T , causing the hopping probability exponential to fall at high T and causing the conductivity maximum. It may be that the Arrhenius prefactor A is rising in this temperature range, as we had speculated for BiCl_3 , but this need not be the case; a recipe for appropriate apportioning of rising E_a vs. falling A during expansion is not yet known. To merely offer a tangible

TABLE V. Specific conductivities ($\Omega^{-1} \text{cm}^{-1}$) from exemplary density-dependent Arrhenius equations (Eq. (1), with $E_a(\rho)$ and $A(\rho)$ given in the text), compared to experimental values from Ref. 14.

T (K)	$\sigma(\text{SnCl}_2)$ expt	$\sigma(\text{SnCl}_2)$ equation	% error	T (K)	$\sigma(\text{HgBr}_2)$ expt	$\sigma(\text{HgBr}_2)$ equation	% error
529	0.803	0.857	6.8	528	0.000 166	0.000 161	-3.2
560	1.028	1.025	-0.2	538	0.000 183	0.000 180	-1.8
598	1.259	1.236	-1.8	579	0.000 259	0.000 259	-0.1
620	1.376	1.357	-1.3	618	0.000 322	0.000 326	1.2
656	1.578	1.553	-1.6	620	0.000 324	0.000 329	1.5
682	1.710	1.689	-1.2	653	0.000 368	0.000 370	0.5
729	1.938	1.921	-0.9	664	0.000 380	0.000 380	-0.1
776	2.127	2.129	0.1	698	0.000 402	0.000 397	-1.3
781	2.147	2.150	0.1	729	0.000 406	0.000 396	-2.5
834	2.330	2.349	0.8	756	0.000 396	0.000 383	-3.2
879	2.467	2.489	0.9	804	0.000 351	0.000 342	-2.7
929	2.587	2.614	1.1	826	0.000 318	0.000 317	-0.3
978	2.676	2.706	1.1	853	0.000 281	0.000 284	1.2
1034	2.755	2.775	0.7			<i>rms % error</i>	1.8
1081	2.796	2.807	0.4				
1132	2.814	2.817	0.1				
1154	2.815	2.814	0.0				
1158	2.815	2.813	-0.1				
1183	2.809	2.804	-0.2				
1213	2.790	2.788	-0.1				
1235	2.772	2.771	0.0				
		<i>rms % error</i>	1.7				

example, the choice of $E_a(\rho) = 35.947 - 16.766 \rho + 2.221 \rho^2$ (kcal mol⁻¹) and $A = 75$ (Ω⁻¹ cm⁻¹) for Eq. (1), together with the SnCl₂ ρ-to-T conversion (Eq. (2)), fits the experimental data extremely well (Table V).

We next address the molecular covalent case, $\sigma_{\text{HgBr}_2}(T)$. Here the density is sufficiently sparse that the halide atoms are usually 1-coordinate, with frequent episodes of intermolecular collision, occasionally resulting in metathesis exchange of halide. Free bromide ions are apparently briefly present (Table III) but short-lived and never far away from a mercury atom in this melt. In the observed Grotthuss chain, the bromide hops from Hg to Hg required a properly oriented “collision” event and, when such an event occurred, the hopping distance seemed somewhat consistent from hop to hop. It would therefore seem more reasonable to ascribe the Grotthuss effect here as Geirer and Wirtz⁴⁸ imagined doing for aqueous acids in H₂O (discussed above): with a loss of collision frequency during thermal expansion. Hence we suggest that *in molecular covalent molten halides, the Grotthuss nature of halide conductivity adds negative curvature to $\sigma(T)$ by providing a falling Arrhenius prefactor A during thermal expansion*, causing the conductivity maximum. As with SnCl₂, a recipe for apportioning a rising E_a vs. falling A during expansion of molten HgBr₂ is not yet known, but as a tangible example the choice of $E_a = 14.35$ (kcal mol⁻¹) and $A(\rho) = (2.7 \times 10^{-8}) e^{4.417 \rho}$ (Ω⁻¹ cm⁻¹) for Eq. (1), together with the HgBr₂ ρ-to-T conversion (Eq. (3)), fits the experimental data extremely well (Table V).

V. CONCLUSIONS

Simulations, employing atomic forces computed with DFT PW91 with an added van-der-Waals attractive potential, qualitatively (and with correct order of magnitude) reproduced the conductivity maxima vs. temperature for molten SnCl₂ and molten HgBr₂.

Molten SnCl₂, like BiCl₃, is (in the simulations) a network covalent liquid with bridging-chloride structure. Molten HgBr₂, with a conductivity lower than SnCl₂ by three orders of magnitude, is an interesting molecular covalent liquid, whose linear triatomic molecules undergo frequent dimeric collisions (1 per 5 ps per molecule), many producing metathesis exchange of bromide ions. The simulations of molten HgBr₂ show autoionization equilibria, but each individual ion (of which Br⁻ is most common) has only a picosecond lifetime. The concentration of these short-lived ions is predicted by the simulations to steadily increase with temperature, in disagreement with the long-standing ion association explanation for the conductivity maximum.

In the molten HgBr₂ simulations, clear Grotthuss mechanisms of bromide ions are seen. An artificial Grotthuss “lock,” a Grotthuss chain to a replicant of the originating molecule, was located and shown to contribute to artificially high conductivity predictions. Time segments showing such conductivity spikes were discarded from the data averaging during conductivity calculation.

Given the lack of support for the ion association hypothesis from the simulations, and instead the observance of a Grotthuss mechanism of halide ions in HgBr₂, we feel that

further pursuance of Grotthuss ideas in understanding molten salt conductivity at high temperatures is the appropriate way to interpret conductivity maxima vs. temperature. The effect of the Grotthuss mechanism in various systems was explored. In aqueous acids, the effect is to cause a negative curvature in $\sigma(T)$ simply due to the reduction of the activation energy for H⁺ mobility. In network covalent molten halides, the Grotthuss effect could be a rise in activation energy as the liquid expands during heating, due to increased halide hopping distance, with the rise at a sufficient pace as to cause a conductivity maximum vs. temperature. Finally, in molecular covalent molten halides, the Grotthuss effect could instead be a drop in intermolecular collision frequency as the liquid expands during heating, with the drop at a sufficient pace as to cause a conductivity maximum vs. temperature.

ACKNOWLEDGMENTS

This work was supported by the Natural Sciences and Engineering Research Council (Discovery Grant No. 238871-2012), with supercomputer funding from the Canada Foundation for Innovation (Leading Edge Fund 2009, Grant No. 21625), and the Government of Saskatchewan Innovation and Science Fund. The Laboratory of Computational Discovery (Robert Cowles, sysadmin) is thanked for supercomputer upkeep.

APPENDIX: THE ORIGINAL EXPERIMENTS

Here we comment on the unlikelihood of experimental artefacts causing the conductivity maxima in the experiments of Grantham and Yosim.¹⁴ (i) One argument against such artefacts causing the conductivity maxima is that the simulations (which are absent of such effects) also produce the conductivity maxima. (ii) Faradaic rectification (in alternating-current mode) and electrode deposit effects (in direct-current mode or from faradaic rectification) are assumed to be absent in the Grantham and Yosim experiments, since their first experiments (involving BiI₃) were performed three ways (2-electrode alternating current, and 4-probe and 2-probe direct current), all producing common conductivity values to within 0.1%.⁵⁷ Any potentially insulating deposits are expected to be *less* stable at the elevated temperatures where conductivity begins to fall; for instance, a hypothetical Hg₂Br₂ deposit would decompose near 345 °C,⁵¹ *before* the conductivity fall. (iii) Effects due to loss of liquid to the vapour phase (e.g., coupled equilibria of the type ionic/molecular with liquid/vapour) are difficult to imagine. It is true that a maximum in concentration is possible with coupled equilibria in a *homogeneous* phase (all solutes or all gases): for example, if one considers $C \rightleftharpoons A$ and $C \rightleftharpoons D$ with equilibrium constants $K_1 = e^{-1000/T}$ and $K_2 = 10 e^{-3000/T}$, the mole fraction of A passes through a maximum at $T = 1001$ K. However, in a *heterogeneous* situation where $C \rightleftharpoons D$ is a liquid vapour equilibrium, the mole fraction of A (e.g., ions) cannot pass through a maximum. This is because the amount of vapour D is independent of how much liquid C is present, leaving the mole fraction of A independent of K_2 and monotonically dependent upon K_1 , which itself is monotonically dependent

on T. As an example, if one considers $C_{\text{liq}} \rightleftharpoons A^+_{\text{liq}} + B^-_{\text{liq}}$ and $C_{\text{liq}} \rightleftharpoons C_{\text{vap}}$ with equilibrium constants $K_1 = e^{-1000/T}$ and $K_2 = p_{C^*}$ (vapour pressure of pure C, independent of excess amount C), then

$$\begin{aligned} x_A &= \frac{1}{2} K_1 \left(-1 + \sqrt{1 + 4K_1^{-1}} \right) \\ &= \frac{1}{2} e^{-1000/T} \left(-1 + \sqrt{1 + 4e^{1000/T}} \right), \end{aligned} \quad (\text{A1})$$

which has no maximum, monotonically rising to $x_A \rightarrow \frac{1}{2} (-1 + \sqrt{5}) = 0.618$ as $T \rightarrow \infty$. Furthermore, we remind the reader that any ion/molecule equilibrium present may have little relevance for molten salt conductivity because the conductivity mechanism is concluded to be a Grotthuss one, where *all* halide ions (bonded or not) have contributing mobility.

- ¹J. Dupont, *Acc. Chem. Res.* **44**, 1223 (2007).
²G. J. Janz, C. Solomons, and H. J. Gardner, *Chem. Rev.* **58**, 461 (1958).
³B. J. Piersma, D. M. Ryan, E. R. Schumacher, and T. L. Riechel, *J. Electrochem. Soc.* **143**, 908 (1996).
⁴C. A. Dos Santos and E. J. Pessine, *Proc. Electrochem. Soc.* **98**(11), 98 (1998).
⁵X. Y. Yan and D. J. Fray, *J. Alloys Compd.* **486**, 154 (2009).
⁶S. Sanchez, C. Lucas, G. S. Picard, M. R. Bermejo, and Y. Castrillejo, *Thin Solid Films* **361**, 107 (2000).
⁷J. Wei, Q. Guo, X. Li, and B. Li, *J. Mater. Sci.* **50**, 4952 (2015).
⁸R. A. Guidotti and P. Masset, *J. Power Sources* **161**, 1443 (2006).
⁹K. Wang, K. Jiang, B. Chung, T. Ouchi, P. J. Burke, D. A. Boysen, D. J. Bradwell, H. Kim, U. Muecke, and D. R. Sadoway, *Nature* **514**, 348 (2014).
¹⁰B. L. Spatocco, T. Ouchi, G. Lambotte, P. J. Burke, and D. R. Sadoway, *J. Electrochem. Soc.* **162**, A2729 (2015).
¹¹K. E. Johnson, *Electrochem. Soc. Interface* **16**, 38 (2007).
¹²G. W. Driver and K. E. Johnson, *ECS Trans.* **16**(49), 19 (2009).
¹³L. F. Grantham and S. J. Yosim, *J. Phys. Chem.* **67**, 2506 (1963).
¹⁴L. F. Grantham and S. J. Yosim, *J. Chem. Phys.* **45**, 1192 (1966).
¹⁵L. F. Grantham and S. J. Yosim, *J. Phys. Chem.* **72**, 762 (1968).
¹⁶A. J. Darnell, W. A. McCollum, and S. J. Yosim, *J. Phys. Chem.* **73**, 4116 (1969).
¹⁷B. F. Markov and Yu. K. Delimarskii, *Ukrain. Khim. Zhur.* **19**, 255 (1953).
¹⁸G. J. Janz and J. D. E. McIntyre, *Ann. N. Y. Acad. Sci.* **79**, 790 (1960).
¹⁹G. J. Janz and J. D. E. McIntyre, *J. Electrochem. Soc.* **109**, 842 (1962).
²⁰G. J. Janz and D. W. James, *J. Chem. Phys.* **38**, 905 (1962).
²¹G. Treiber and K. Tödheide, *Ber. Bunsen-Ges. Phys. Chem.* **77**, 540 (1973).
²²K. Tödheide, *Angew. Chem., Int. Ed. Engl.* **19**, 606 (1980).
²³A. T. Clay, C. M. Kuntz, K. E. Johnson, and A. L. L. East, *J. Chem. Phys.* **136**, 124504 (2012).
²⁴C. M. Kuntz and A. L. L. East, *ECS Trans.* **50**(11), 71 (2013).
²⁵C. J. T. de Grotthuss, *Ann. Chim. Phys.* **58**, 54 (1806); English translations appeared as, C. J. T. de Grotthuss, *Philos. Mag. Ser. 1* **25**, 330 (1806); and as C. J. T. de Grotthuss, *Biochim. Biophys. Acta* **1757**, 871 (2006).
²⁶T. Erdey-Grúz, *Z. Phys. Chem. A* **178**, 138 (1937).
²⁷For molten TiCl, see, P. L. Spedding, *J. Phys. Chem.* **76**, 1348 (1972); *Electrochim. Acta* **18**, 111 (1973); For I⁻/I₂, see, D. J. Bearcroft and N. H. Nachtrieb, *J. Phys. Chem.* **71**, 316 (1967); *ibid.* **71**, 4400 (1967); For Br⁻/Br₂, see, I. Rubenstein, M. Bixon, and E. Gileadi, *J. Phys. Chem.* **84**, 715 (1980); For a very recent report of O²⁻ shuttling in a simulation of CO₂ in molten CaCO₃, see, D. Corradini, F.-X. Coudert, and R. Vuilleumier, *Nat. Chem.* **8**, 454 (2016).
²⁸G. Kresse and J. Hafner, *Phys. Rev. B* **47**, 558 (1993).
²⁹G. Kresse and J. Furthmüller, *Phys. Rev. B* **54**, 11169 (1996).
³⁰G. Kresse and J. Hafner, *J. Phys.: Condens. Matter* **6**, 8245 (1994).
³¹G. Kresse and D. Joubert, *Phys. Rev. B* **59**, 1758 (1999).
³²S. Nosé, *J. Chem. Phys.* **81**, 511 (1984).
³³A. R. Leach, *Molecular Modelling: Principles and Applications*, 2nd ed. (Pearson, Harlow, UK, 2001).
³⁴W. Humphrey, A. Dalke, and K. Schulten, *J. Mol. Graphics* **14**, 33 (1996).
³⁵D. D. Koelling and B. N. Harmon, *J. Phys. C: Solid State Phys.* **10**, 3107 (1977).
³⁶J. P. Perdew, J. A. Chevary, S. H. Vosko, K. A. Jackson, M. R. Pedersen, D. J. Singh, and C. Fiolhais, *Phys. Rev. B* **46**, 6671 (1992).
³⁷S. Grimme, *J. Comput. Chem.* **27**, 1787 (2006).
³⁸G. J. Janz, *J. Phys. Chem. Ref. Data* **17**(Suppl. 2), 1–309 (1988).
³⁹D. Coslovich, J.-P. Hansen, and G. Kahl, *J. Chem. Phys.* **134**, 244514 (2011).
⁴⁰M. J. Frisch, G. W. Trucks, H. B. Schlegel, G. E. Scuseria, M. A. Robb, J. R. Cheeseman, G. Scalmani, V. Barone, B. Mennucci, G. A. Petersson, H. Nakatsuji, M. Caricato, X. Li, H. P. Hratchian, A. F. Izmaylov, J. Bloino, G. Zheng, J. L. Sonnenberg, M. Hada, M. Ehara, K. Toyota, R. Fukuda, J. Hasegawa, M. Ishida, T. Nakajima, Y. Honda, O. Kitao, H. Nakai, T. Vreven, J. A. Montgomery, Jr., J. E. Peralta, F. Ogliaro, M. Bearpark, J. J. Heyd, E. Brothers, K. N. Kudin, V. N. Staroverov, R. Kobayashi, J. Normand, K. Raghavachari, A. Rendell, J. C. Burant, S. S. Iyengar, J. Tomasi, M. Cossi, N. Rega, J. M. Millam, M. Klene, J. E. Knox, J. B. Cross, V. Bakken, C. Adamo, J. Jaramillo, R. Gomperts, R. E. Stratmann, O. Yazyev, A. J. Austin, R. Cammi, C. Pomelli, J. W. Ochterski, R. L. Martin, K. Morokuma, V. G. Zakrzewski, G. A. Voth, P. Salvador, J. J. Dannenberg, S. Dapprich, A. D. Daniels, Ö. Farkas, J. B. Foresman, J. V. Ortiz, J. Cioslowski, and D. J. Fox, *GAUSSIAN 09, Revision C.01*, Gaussian, Inc., Wallingford, CT, 2009.
⁴¹K. Hilpert, S. Roszak, J. Saloni, M. Miller, P. Lipkowski, and J. Leszczynski, *J. Phys. Chem. A* **109**, 1286 (2005).
⁴²J. M. van den Berg, *Acta Crystallogr.* **14**, 1002 (1961).
⁴³A. B. Salyulev and A. M. Potapov, *Z. Naturforsch.* **70a**, 683 (2015).
⁴⁴J. M. R. Clarke and C. Solomons, *J. Chem. Phys.* **47**, 1823 (1967).
⁴⁵J. O'M. Bockris and A. K. N. Reddy, *Modern Electrochemistry* (Plenum Press, New York, 1970), Vol. 1.
⁴⁶J. Johnston, *J. Am. Chem. Soc.* **31**, 1010 (1909).
⁴⁷T. Erdey-Grúz, *Transport Phenomenon in Aqueous Solutions* (Halsted Press, John Wiley & Sons, Inc., New York, 1974).
⁴⁸A. Gierer and K. Wirtz, *J. Chem. Phys.* **17**, 745 (1949); A. Gierer and K. Wirtz, *J. Phys. Chem.* **56**, 914 (1952).
⁴⁹B. E. Conway, J. O'M. Bockris, and H. Linton, *J. Chem. Phys.* **24**, 834 (1956).
⁵⁰H. Bloom and E. Heymann, *Proc. R. Soc. A* **188**, 392 (1947).
⁵¹*CRC Handbook of Chemistry and Physics*, 96th ed., edited by W. M. Haynes (CRC Press, Boca Raton, FL, 2015), Sec. 4, pp. 4–43.
⁵²A. Klemm, "Transport properties of molten salts," in *Molten Salt Chemistry*, edited by M. Blander (InterScience, New York, 1964).
⁵³A. B. Salyulev and A. M. Potapov, *J. Chem. Eng. Data* **60**, 484 (2015).
⁵⁴C. A. Angell, *J. Phys. Chem.* **70**, 2793 (1966).
⁵⁵S. I. Smedley, *The Interpretation of Ionic Conductivity in Liquids* (Plenum Press, New York, 1980).
⁵⁶I. Okada and R. Takagi, *Z. Naturforsch.* **36a**, 378 (1981).
⁵⁷L. F. Grantham and S. J. Yosim, *J. Chem. Phys.* **38**, 1671 (1963).